The Biomechanics of the Pediatric and Adult Human Thoracic Spine

Francisco J. Lopez-Valdes, Sabrina Lau, Patrick Riley, John Lamp, Richard Kent
University of Virginia – Center for Applied Biomechanics

ABSTRACT – A growing body of literature points out the relevance of the thoracic spine dynamics in understanding the thorax-restraint interaction as well as in determining the kinematics of the head and cervical spine. This study characterizes the dynamic response in bending of eight human spinal specimens (4 pediatric: ages 7 and 15 years, 4 adult: ages 48 and 52 years) from two sections along the thoracic spine (T2-T4 and T7-T9). Each specimen consisted of three vertebral bodies connected by the corresponding intervertebral discs. All ligaments were preserved in the preparation with the exception of the inter-transverse ligament. Specimens were exposed to a series of five dynamic bending ramp-and-hold tests with varying amplitudes at a nominal rate of 2 rad/s. After this battery of tests, failure experiments were conducted. The 7-year-old specimen showed the lowest tolerance to a moment (T2-T4: 12.1 Nm; T7-T9: 11.6 Nm) with no significant reduction of the relative rotation between the vertebrae. The 15-year-old failure tolerance was comparable to that of the adult specimens. Failure of the adult specimens occurred within a wide range at the T2-T4 thoracic section (23.3 Nm- 53.0 Nm) while it was circumscribed to the interval 48.3 Nm-52.5 Nm for the T7-T9 section. The series of dynamic ramp-and-hold were used to assess two different scaling methods (mass scaling and SAE scaling). Neither method was able to capture the stiffness, peak moment and relaxation characteristics exhibited by the pediatric specimens.

INTRODUCTION

Head injuries are the most severe and frequent injuries found in motor vehicle crashes. The kinematics of the head/neck complex as well as the interaction between the torso of the occupants and the restraint are dictated by the dynamic behavior of the thoracic spine (Alem et al., 1978). The spine can also be damaged in a crash resulting in a high risk of associated morbidity and mortality (Nahum and Melvin, 2002; Holmes, 2001; Hu et al., 1996) or on minor injuries causing chronic pain (Pape et al., 2007; Spitzer et al., 1995).

Recent studies combining full sled tests and computer simulations have found significant differences in the magnitudes of the acceleration at T1 and the neck loads between Anthropomorphic Test Devices (ATD) and cadavers (Shaw et al., 2000, 2001; Lopez-Valdes et al., 2010). Other studies have shown similar findings in pediatric ATD (Sherwood et al., 2003; Ash et al., 2009; Lopez-Valdes et al., 2009). Clearly, if the original adult-size ATD does not describe correctly the kinematics of the human, the scaled pediatric version could not achieve this goal either. Arbogast et al. (2009) characterized head and spinal motion of pediatric and adult volunteers in a non-injurious low-speed simulated frontal impact showing that the flexion angle of the pediatric thoracic spine was significantly greater than that of the adult one.

CORRESPONDING AUTHOR: Francisco J. Lopez-Valdes, BEng, Center for Applied Biomechanics, University of Virginia. 4040 Lewis and Clark Drive, Charlottesville, VA 22911, USA; Email: fjl2j@virginia.edu

Another study comparing the abdominal and chest force-deflection characteristics between pediatric and adult Post Mortem Human Subjects (PMHS) showed that the predicted pediatric response given by several commonly used scaling methods failed to predict the actual pediatric response (Kent et al., 2009). Both studies suggest that while scaling is still an important tool in the development of physical and computational models, any actual pediatric data that can guide the scaling process should be considered.

Although there is a substantial body of literature discussing the biomechanics of the thoracic spine, the great majority of the studies belong to the field of orthopedics and orthotics. The application of these studies to the prevention of motor-vehicle related injuries is limited (Sran et al., 2005; Anderson et al., 2009). A few studies have attempted the mechanical characterization of the healthy cadaveric thoracic spine in bending (Markolf, 1970; Panjabi et al., 1976) only in quasi-static conditions. More recently, Willems et al. (1996) measured the *in-vivo* 3D kinematics of the human thoracic spine, but again in quasi-static conditions. The study showed that quasi-static flexion and extension were relatively pure plane motions, accompanied by slight axial rotation. Current literature is lacking in experimental data on the dynamic behavior of the human thoracic spine that can assist in the development of FE models of the spine as well as a more biofidelic ATD spine.

This paper presents the results obtained from the dynamic testing of two sections of the human thoracic spine in bending, which is the predominant

loading mechanism that a car occupant's spine undergoes in a frontal impact. To the knowledge of the authors, this is the first time that dynamic data from human thoracic specimens have been published. The specific goals of the paper are the following:

- To compare the tolerance to bending between human pediatric and adult thoracic spines.
- To assess the validity of two of the most-used scaling paradigms (mass scaling, SAE scaling) to scale the response of the adult human thoracic spine.

METHODS

Experiment setup

A custom-made fixture specifically designed to induce rotation of a section of the spine in the sagittal plane was attached to a servohydraulic testing machine (INSTRON 8874 Axial-Torsion Fatigue Testing Systems, Norwood, MA, USA). The fixture was driven by the vertical motion of the piston of the machine, transforming the linear motion into a rotation of two cups through a mechanical linkage. The assembly consisted of two aluminum links joined by a low-friction rotational bearing. The vertical link was attached to the crosshead of the testing machine by a low-friction linear bearing. The cups were supported by two cup-holders that could translate with no friction in the horizontal plane of the table of the test machine (Figure 1). A global coordinate system (GCS) rigidly attached to the table of the test machine was defined as shown in Figure 1.

Preparation of the specimens

For the purpose of this study, a Functional Spinal Unit (FSU) was defined as the segment formed by three vertebral bodies, the corresponding two inter-vertebral discs and the ligaments connecting these structures. All the ligaments (supra-spinous (SSL), inter-spinous (ISL), flavum (LF), posterior longitudinal (PLL), anterior longitudinal (ALL)) were preserved during the preparation of the specimens with the exception of the inter-transverse ligaments. Two FSU were obtained from each thoracic spine: T2-T4 and T7-T9. A total of eight FSU were harvested from four donors (two pediatric, two adults). The anthropometry and general characteristics of the donors are shown in Table 1. The extraction, preparation and testing of the specimens were made in compliance with the Protocol for the Handling of Biological Material (Center for Applied Biomechanics, 2006) and approved by the University of Virginia – Center for Applied Biomechanics Oversight Committee.

Table 1. Characteristics of the PMHS

Subject	Gender	Age	Stature (cm)	Weight (kg)
F470	Female	7	119	27
M485	Male	15	163	50
M319	Male	52	179	77
M320	Male	48	168	68

The proximal and distal vertebrae of each FSU were embedded into cement (Fast Cast, polyurethane isocyanate, Goldenwest Inc., CA, USA). A custom-made potting fixture was used to ensure that the two cement blocks were aligned without inducing any initial stress in the specimens. The center of the potted vertebral bodies was approximately positioned at the center of the cement block.

The specimens were kept frozen and thawed 24 hours prior to testing. To preserve the hydration of the ligamentous structure they were wrapped in gauze soaked in saline solution. The specimens were submerged in a temperature controlled bath set at 37.1 degrees Celsius for at least 30 minutes immediately prior to testing.

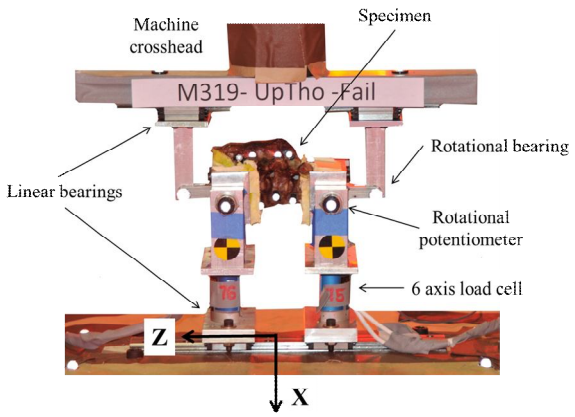

Figure 1. Schematic showing the test setup, instrumentation and positioning of the specimen on the test rig.

Instrumentation

Motion capture system. The relative motion of the vertebrae was tracked using an 8-camera Vicon MX™ system operating at 1,000 Hz. The system recorded the motion of retroreflective targets within the camera's collective viewing volume. Four targets were glued onto each vertebra to allow for the reconstruction of their 3D motion. A local coordinate system located at the center of the vertebral body was defined for each vertebra (Wu et al., 2005). Using geometric information from CT images, the position

and attitude of the local coordinate system can be related to the position of the four retroreflective targets. A calibration procedure, performed prior to testing each specimen, estimated the optical characteristics of each camera and established its position and orientation in a reference coordinate system. With this information a photogrametric algorithm within the Vicon Nexus software package reconstructed the 3D position of each target for each video sample increment from the multiple 2D camera images. Finally, following the method described in Kinzel et al. (1972), the 6-degrees-of-freedom motion of each vertebra can be determined with respect to an inertial global coordinate system (GCS) that coincides with the base of the test machine.

Other non-optical instrumentation. Two load cells (Implantable Fibula, Model No. 5024J, Robert A. Denton, Inc. MI, USA) measured the reaction forces and moments experimented by the support of the cups in the three coordinate axes. The longitudinal axis of the load cells intersected perpendicularly with the axis of rotation of the cups. The rotation of the cups was measured by two rotational potentiometers. Instrument data were collected at 10,000 Hz using a DEWE-2600 (Dewetron Inc., Wakefield, RI, USA) data acquisition system. The data were later filtered again using a low-pass CFC100 (rotational potentiometers) and CFC1000 filters (forces and moments).

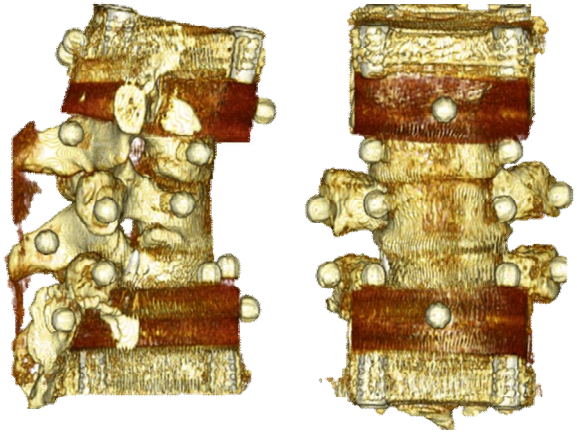

Figure 2. CT images showing the position of the markers on the FSU (M320-T1-T5).

Test procedures

Each specimen was exposed to a series of dynamic tests. First, a battery of 50 cycles at 1 Hz sinusoid with different amplitudes was applied to precondition the tissue and achieve a steady-state behavior. Next, a series of five dynamic ramp and 60-second hold tests of varying amplitudes were applied to the specimens. The amplitude of the ramps was chosen to avoid causing any damage to the tissue and the maximum amplitude reached during the dynamic tests was similar to that reached during the preconditioning of the tissue. The piston of the test machine moved upwards at a nominal rate of 100 mm/s which caused an angular rate in the cups of approximately 2 rad/s. Finally, specimens were exposed to a dynamic ramp (with amplitudes varying from 11.7 to 20.6 degrees) to cause the failure of the tissue.

Table 2 summarizes the test matrix as well as the machine input values of each of the tests. The values of the amplitudes presented in the table correspond to the rotation of the cups as measured by the rotational potentiometers.

Analyses of the data

Two different sets of results are included in this paper. First, the tolerances of the pediatric and adult thoracic FSU to an applied rotation are presented and compared. Second, two commonly used scaling methods (mass scaling, SAE scaling) were applied to the dynamic responses of selected adult specimens and were compared to the actual response of the pediatric FSU.

Scaling methods

Two scaling paradigms are used and discussed in this paper. Given the small sample size available, and instead of averaging the responses of the adult and pediatric subjects, it was decided to analyze how these two methodologies worked when they were applied to one of the adult subjects (M320) to predict the response of the pediatric subject F470.

Mass scaling. The method was first used in Eppinger et al. (1984). It is based on dimensional analysis and assumes that there is geometrical and dynamic similarity between the two systems related by the scaling method. The three fundamental magnitudes that are used to scale all the other magnitudes in the system are length (subscript L), mass density (subscript ρ) and modulus of elasticity (subscript E). A length scale factor is calculated as the cube root of the ratio of the mass (subscript m) of a standard-sized subject to the actual subject, assuming that the densities are equal between the subjects. The difference in material properties due to tissue development are accounted for in this method according to the value λ_E proposed in Table 3. In the original study λ_E was assumed to be 1 (Eppinger et al., 1884), since it dealt with scaling between different sizes of adults. More recent studies such as

Mertz et al. (2003) reported the ratio of elastic moduli of tendons (λ_{EB}=0.88) between a 6-year-old and an adult mid-size male to be used to scale the mechanical response of the adult. Though this value was originally proposed to be used within the SAE scaling paradigm, it has been considered also here to account for the differences in tissue properties due to development. The following relationships can be derived using dimensional analysis:

$$\lambda_t = \lambda_E^{-1/2}\lambda_m^{1/3} \quad \text{Equation 1}$$

$$\lambda_M = \lambda_E\lambda_m \quad \text{Equation 2}$$

where t is the time and M is the moment.

SAE scaling. This method was originally applied to scale the Hybrid III 50th percentile to the small female and large male ATD. The method involves a length scale factor λ_z (given by the erect seated height of the subjects) and a mass scale factor (total body mass). Again the assumption of equal density is imposed in the method, so that the length scale factors in the x- and y- directions are given by Equation 3.

$$\lambda_x = \lambda_y = \sqrt{\frac{\lambda_m}{\lambda_z}} \quad \text{Equation 3}$$

The SAE scaling method also considers the differences in the material properties of the tissue due to maturation. These differences are given by the scaling factor for the modulus of elasticity λ_E shown in Table 3 (Mertz et al., 2003). Mertz et al. (1989) developed the following expressions to scale the bending moment/angle response of the neck between different sizes of adults:

$$\lambda_\theta = \lambda_z/\lambda_x \quad \text{Equation 4}$$

$$\lambda_M = \lambda_E\lambda_x\lambda_y\lambda_x = \lambda_E\lambda_x^3 \quad \text{Equation 5}$$

In the original work in Mertz et al. (1989), λ_E was assumed to be equal to 1 since the scaling was applied to adult subjects. In this study, the moment-scaling factor has been updated to reflect the age-changing properties of the tissue as shown in Table 3 (λ_E=0.667).

Table 2. Test matrix.

Specimen	Preconditioning		D1	D2	D3	D4	D5	Failure	Preconditioning amplitude / Failure amplitude
	Freq (Hz)	# cycles/ Amplitude (deg)	Amplitude (deg)	Amplitude (deg)	Amplitude (deg)	Amplitude (deg)	Amplitude (deg)	Amplitude (deg)	
F470-T2T4	1	10/0.65, 10/1.35, 30/1.89	0.63	0.93	1.22	1.54	1.87	11.72	35%
F470-T7T9	1	10/0.59, 10/1.17, 30/2.00	0.61	0.89	1.15	1.37	1.61	11.77	22%
M485-T2T4	1	10/1.04, 10/2.27, 30/3.39	0.87	1.41	1.95	2.54	3.18	17.60	NA
M485-T7T9	1	10/1.09, 10/2.33, 30/3.44	0.85	1.42	2.00	2.64	3.32	20.10	39%
M319-T2T4	1	10/1.14, 10/2.25, 30/3.35	0.96	1.53	2.13	2.69	3.24	18.27	42%
M319-T7T9	1	10/1.18, 10/2.43, 30/4.64	0.79	2.04	3.35	3.98	4.59	18.52	43%
M320-T2T4	1	10/1.24, 10/2.36, 30/3.41	1.10	1.75	2.43	2.96	3.46	18.75	43%
M320-T7T9	1	10/1.07, 10/2.01, 30/2.97	0.87	1.43	2.04	2.57	3.10	20.60	56%

Table 3. Scaling factors between specimens M320-T7T9 and F470-T7T9 as given by the mass scaling and the SAE scaling methods.

	λ_L	λ_ρ	λ_E	λ_m	λ_t	λ_M	λ_θ
Mass scaling	λ_x=λ_y=λ_z=0.73	1	0.880	0.40	0.79	0.35	1
SAE scaling	λ_z=0.71, λ_x=λ_y=0.75	1	0.667	0.40	1	0.28	0.95

RESULTS

The test fixture transformed the longitudinal translation of the piston of the axial machine into a rotation of the cups attached to the two ends of the specimens. Therefore, both the range of the applied angles as well as the angular rate were specimen dependent. Given the rate dependent nature of most biological tissues, it was important to assure that the angular rate between specimens was similar. Figure 3 compares the responses of one pediatric and one adult specimen, showing no differences between the applied angular rates. Figure 4 and Figure 5 show the results obtained during the preconditioning of one pediatric and one adult FSU.

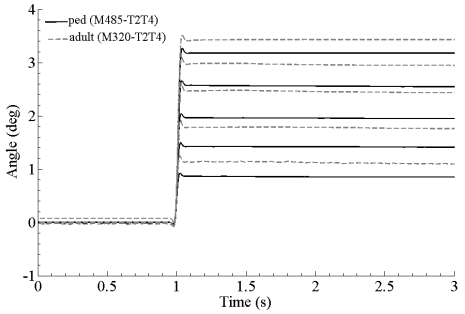

Figure 3. Angle vs. time in the dynamic ramp-and-hold tests. The angular rate applied to the pediatric and adult specimens was nominally the same.

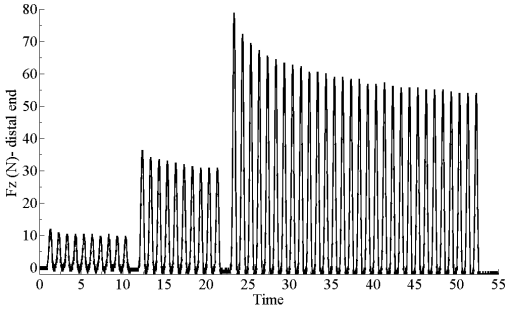

Figure 4. Preconditioning of pediatric specimen (F470 T7-T9).

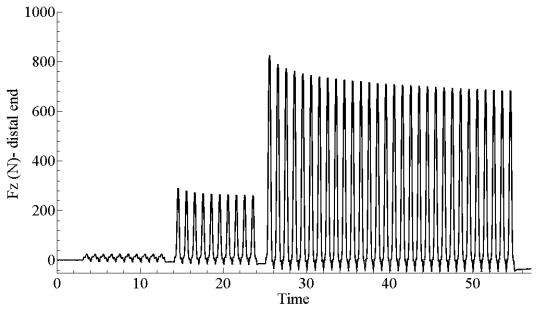

Figure 5. Preconditioning of adult specimen (M320 T7-T9).

Failure tests

The failure tests consisted of a dynamic ramp performed at nominally 2 rad/s. The amplitude of the ramp varied for each specimen according to the input values shown in Table 2. Figure 6a-h presents the moment time history corresponding to each specimen. Given the dynamic nature of the load applied to the specimens and the anatomical and structural differences between the upper and lower joints, the magnitudes of the moment measured at the two ends of the specimens were different. Table 4 summarizes the values of the moments observed at the time of failure at both ends of the specimens, the time of failure, the relative rotations between the two extreme vertebrae and the central one at failure and the location and type of injury observed (see also Appendix II).

The youngest specimen (F470) exhibited the lowest tolerance. The upper thoracic FSU failed at a moment M=12.1 Nm measured at the superior vertebra and the mid-thoracic section failed at M=8.6 Nm also at the superior end. The relative rotations between the vertebrae at failure were similar in the segment T2-T4 but the superior relative rotation was almost twice the one observed at the inferior joint in the case of the segment T7-T9. Failure of the specimens involved complete tear of the interspinous and supraspinous ligaments as well as partial or complete facet dislocation. The flavum ligament was also torn in the T7-T9 specimen.

The failure moments observed for the other pediatric specimen were not substantially different than the ones exhibited by the adult ones. In the case of M485 T2-T4 the data traces do not show a sudden drop in the value of the moment but a more progressive one instead. After the completion of the test, no injury could be found for this specimen, but visual inspection revealed that there was a crack in the cast that explained the drop of the measured moment. As for M485 T7-T9, it was the only specimen in which the inferior relative angle at failure was greater than the superior one (12.6 vs. 5.2 degrees). Moment peak values are presented in Table 4.

Both sections of specimen M319 exhibited a much more homogeneous behavior than any other specimen. The magnitudes of the moment at the inferior and superior ends were similar and there was only a difference of approximately 3 degrees between the relative rotations of the vertebrae forming the FSU. In the case of the T7-T9 section, the motion of the vertebrae could be reconstructed only up to 101 ms, but the failure of the tissue happened before that instant.

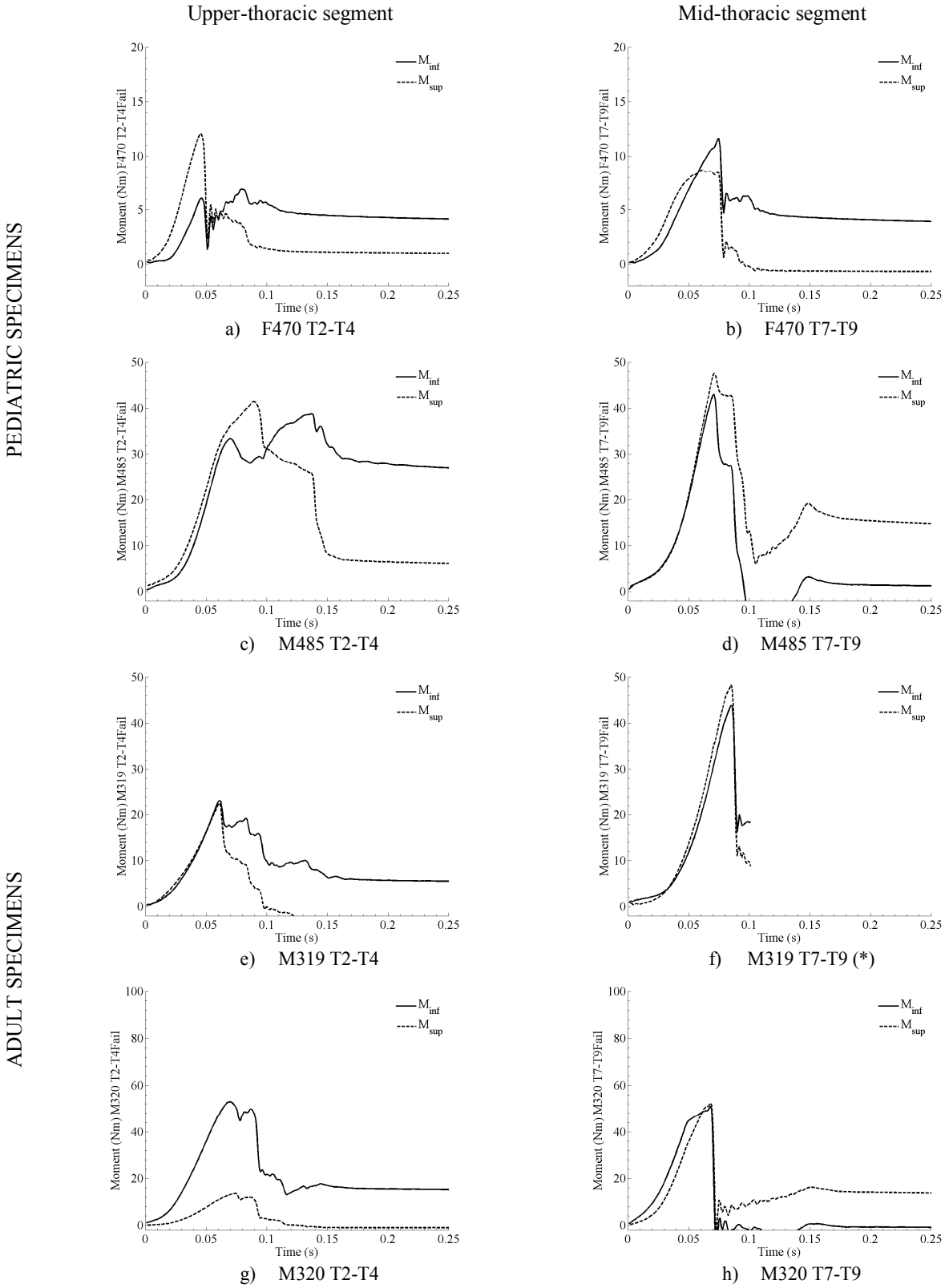

Figure 6 Moment time history in the failure tests estimated at both ends of each specimen. (*) M319 T7-T9 was calculated only up to 0.101 ms as discussed in the text.

Table 4. Moments observed at the superior and inferior locations at the time of failure of the tissue. Relative angles corresponding to the same instant. *: when the two measured moments did not peak at the same time; the reported time corresponds to the marked moment.

	M_{inf} (Nm)	M_{sup} (Nm)	Time (s)	Rel $angle_{inf}$ (deg)	Rel $angle_{sup}$ (deg)	Injury
F470 T2-T4	6.1	12.1	0.046	6.9	7.6	IS and SP T2-T3 complete tear, partial facet dislocation T2-T3
F470 T7-T9	11.6	8.6	0.074	6.6	12.9	IS and SP T7-T8 complete tear, flavum ligament T7-T8, bilateral facet dislocation T7-T8
M485 T2-T4	28.9	41.4*	0.090	10.3	21.0	Superior end cast fractured with no apparent injury.
M485 T7-T9	43.0	47.6	0.071	12.6	5.2	T8-T9 disc rupture, T9 body fracture, PLL rupture at T9 level
M319 T2-T4	23.3	22.6	0.061	6.1	9.3	IS and SP T2-T3 complete tear, flavum ligament torn T2-T3, bilateral facet dislocations T2-T3
M319 T7-T9	43.9	48.3	0.085	9.9	12.1	IS and SP T7-T8 complete tear, flavum ligament T7-T8, bilateral facet dislocation T7-T8
M320 T2-T4	53.0*	13.6	0.07	8.8	10.6	IS and SP T2-T3 complete tear, flavum ligament torn T2-T3, bilateral facet dislocations T2-T3
M320 T7-T9	52.5	51.1	0.068	1.7	15.0	T9 body fracture, partial PLL rupture at T9, T8-T9 disc rupture, partial T8-T9 facet dislocation.

Specimen M320 T2-T4 showed a very low tolerance to the rotation, failing at 13.6 Nm. On the contrary, the T7-T9 section exhibited the highest moment at failure (52.5 Nm). There was an important difference between the moments at the inferior and superior ends of M320 T2-T4 over the whole duration of the test that can be attributed to the extremely thin interspinous ligament at the T2-T3 level observed in this subject. The same behavior was seen during the dynamic ramp-and-hold tests. The weakness of this ligament could explain also the low tolerance to bending in the failure test.

Scaling between specimens

The application of either of the two scaling methods discussed in this paper requires that certain conditions must be satisfied by the specimens related by the scaling process. These requirements are different for each method. Convenient tests verifying the needed characteristics were chosen to show how the scaling methods would predict the response of the pediatric specimens.

The mass scaling method is based on dimensional analysis. Therefore, angles (non-dimensional magnitudes) would remain constant throughout the scaling process to keep the geometrical similarity required by the method. In order to show how this method would work, two different pair of adult/pediatric tests that were subjected to approximate the same relative rotation at the superior joint of the lower FSU (T7-T8) were chosen. These tests are presented in Table 5.

Table 5. Pairs of tests used in the assessment of the mass scaling methods.

Test	Relative superior angle (deg): Adult/Pediatric
M320 T7-T9 D1 F470 T7-T9 D5	2.50/2.50
M320 T7-T9 D2 F470 T7-T9 D4	2.01/2.20

The SAE method scales both the moment and the angle according to the scaling factors shown in Table 3. In this case, the pairs of adult/pediatric tests to be scaled were chosen so that the scaled relative angle rotated by the superior joint of the adult specimen was approximately the same as the relative angle rotated by the same joint of the pediatric FSU. Accordingly, the pairs included in Table 6 were the ones subjected to the SAE scaling methodology.

Figure 7 shows the comparison between the pair of adult/pediatric tests exposed to the same relative rotation and the corresponding scaled adult response

as given by the mass scaling method. Applying the moment scaling factor λ_M=0.35 given in Table 3 would produce an excessive low prediction for the peak moment of the pediatric subject in the first pair of compared tests. However, an accurate prediction of the pediatric peak moment was obtained in the second comparison. Both pediatric specimens exhibited a faster relaxation that was not seen in the adult specimens. This effect was not captured by the scaling process either.

As for the results obtained using the SAE scaling methodology, significant differences were also found between the predicted response of the pediatric specimen and the actual one. When the comparison was done between upper thoracic specimens, it was found that the predicted peak moment and the whole moment response was greater than the one exhibited by the pediatric specimen. The pediatric specimen showed a multi-mode response that was not captured by the scaled adult response. In the case of the superior segment of the thoracic spine, there were not substantial differences between the relaxation characteristics of the specimens. These results are included in Figure 8.

Table 6. Pairs of tests used in the assessment of the SAE scaling methods.

Test	Relative superior angle (deg): Scaled adult/Pediatric
M320 T2-T4 D1 F470 T2-T4 D2	1.44/1.46
M320 T2-T4 D2 F470 T2-T4 D5	2.23/2.23
M320 T7-T9 D1 F470 T7-T9 D4	2.38/2.21

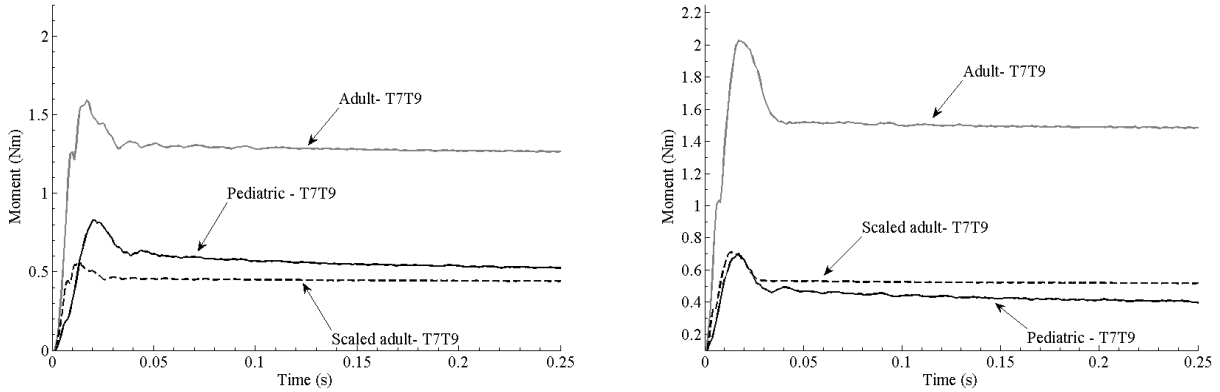

Figure 7 Moment time history comparing adult, pediatric and scaled-adult response given by the mass scaling method (Left: M320 T7-T9 D1 vs. F470 T7-T9 D5. Right: M320 T7-T9 D2 vs. F470 T7-T9 D4).

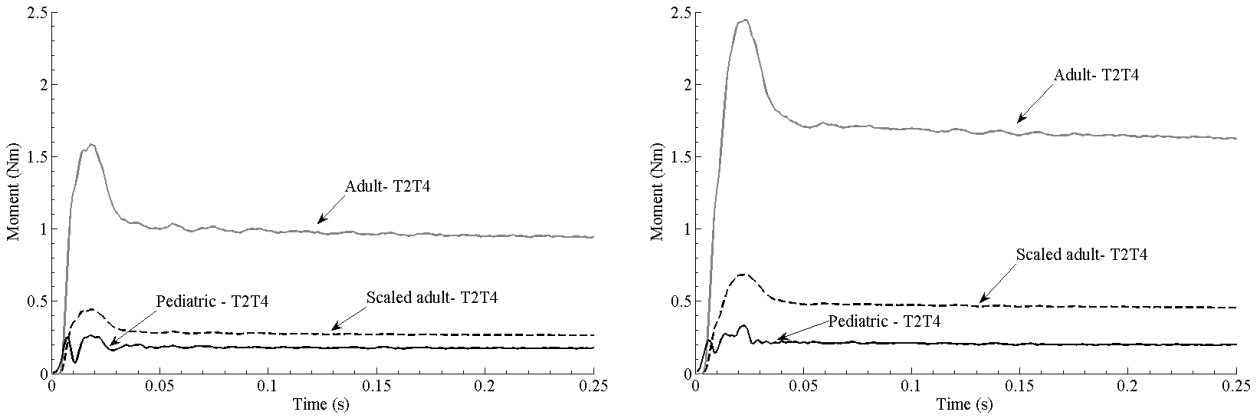

Figure 8 Moment time history comparing adult, pediatric and scaled-adult response given by the SAE scaling method. T2-T4 sections (Left: M320 T2-T4 D1 vs. F470 T2-T4 D2. Right: M320 T2-T4 D2 vs. F470 T2-T4 D5).

The third pair of data compared using the SAE scaling method corresponded to mid-thoracic sections (like the ones used in the mass scaling method). As seen in the case of mass scaling, the predicted pediatric response given by the SAE method was smaller than the actual response of the pediatric specimen. Again, the predicted behavior failed to describe the faster relaxation exhibited by the pediatric specimen. These results are shown in Figure 9.

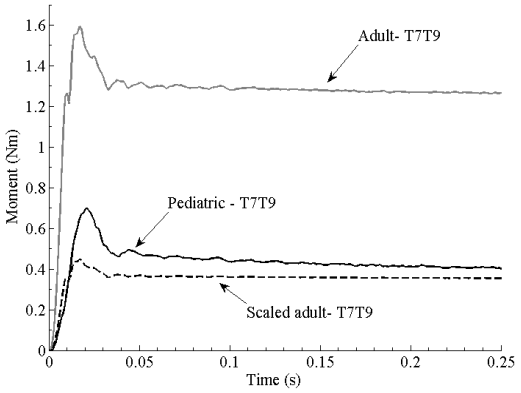

Figure 9 Moment time history comparing adult, pediatric and scaled-adult response given by the SAE scaling method. T7-T9 section. (M320 T7-T9 D1 vs. F470 T7-T9 D4).

DISCUSSION

To our knowledge, this is the first study reporting experimental data of dynamic bending tests of the human thoracic spine. Although the sample size of the study is limited, it also included four pediatric specimens allowing comparison of the mechanical response of the human thoracic spine at several stages of maturity. The different state of ossification of the vertebrae, the change in the orientation of the facet joints and the development of the lordotic curvatures of the spine are some of the changes that occur during maturation that contribute to the differences in behavior between the adult and the pediatric spine in general (Green and Swiontkowski, 1998; Nahum and Melvin, 2002; Franklyn et al., 2007). Two different levels in the thoracic spine T2-T4 and T7-T9) were addressed in this study since previous literature suggested that sagittal plane motion increases in a cephalocaudal direction, consistent with the changing anatomical orientations of the facets moving down along the spine. (Willems et al, 1996). We also observed this phenomenon in all the specimens included discussed here with the exception of M485.

The scarce information available on the bending behavior under dynamic loading of the thoracic spine made the selection of appropriate mechanical inputs to characterize the human thoracic spine difficult. Several studies discussing the behavior of other sections of the spine (McElhaney et al., 1998; Wheeldon et al., 2006; Nightingale et al., 2007; Belwadi and Yang, 2008), studying the behavior of the thoracic spine under quasi-static conditions (Panjabi et al., 1976) and analyzing the change in the range of motion of the thoracic spine after surgical procedures (Sran et al., 2005; Anderson et al., 2009) were combined to obtain an educated guess of the input rotation to be used in the tests discussed in this paper. There was a trade-off between inducing sufficient angle amplitude in the specimens (so that the motion capture system could measure it) and not causing any damage to the tissue during the preconditioning and dynamic tests D1-D5. In the case of the pediatric specimens, the only study found for guidance was a comparison between mature and immature sheep (Clarke et al., 2007). Though the goal of not causing the failure of the tissue during the ramp-and-hold series of tests was successfully achieved, we recommend to use greater amplitudes for the input rotation in future studies, since increased amplitudes will improve the accuracy in the measurement of the relative rotations between the vertebrae.

The opportunity of comparing the responses of pediatric to adult subjects suggested the possibility of assessing two scaling methods that are commonly used in the field of impact biomechanics. Neither of the methods was developed to specifically scale the response of the thoracic spine, but to scale the global response from the 50th percentile adult male dummy to other sizes, including pediatric dummies. However, the important differences found between the spine kinematics of children and adults at low speed (Arbogast et al. 2009) as well as the difficulties in scaling the pediatric thoracic response reported by Kent et al. (2009) motivated us to explore how scaling would work when applied to the thoracic spine. The two scaling methods that were easily transferable to the case of the spine were the mass scaling technique and the SAE method. In this latter case, we borrowed the expressions used to scale the response of the neck and applied them to the thoracic spine instead.

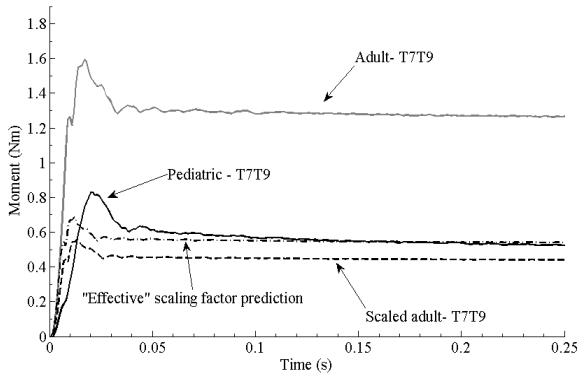

Figure 10 Moment time history comparing adult, pediatric, scaled-adult response given by the mass scaling method and the prediction given by the effective scaling factor for the moment.

A handful of suitable tests to apply these techniques were chosen. Both methods underestimated the pediatric peak response and neither was able to predict the initial stiffness nor the relaxation exhibited by the pediatric specimens. The poor prediction of the pediatric behavior cannot be attributed only to a lack of precision of the value of the scaling factors.

To illustrate the above statement, let us consider the three pairs of tests from the T7-T9 section of M320 and F470 (the adult and the pediatric subjects that have been compared in the previous section). Using the data from these experiments, it is possible to find an effective scaling factor that would provide a better approximation of the peak value of the moment and therefore (given that the angles rotated were the same for the matched tests) a better approximation of the stiffness. The value of the estimated effective scaling factor for the moment is (average ± standard deviation) λ_{Meff}=0.43±0.09. For illustration purposes, Figure 10 shows the improved prediction of the pediatric response using the average value of λ_{Meff} and comparing it with the one obtained by the mass scaling method (the situation for the SAE method would be analogous). However, if the value for the scaling factor of the moment λ_M is made equal to λ_{Meff} then the corresponding individual scaling factors for the module of elasticity given by the mass scaling and the SAE scaling method would be given by the following expressions:

- Mass scaling: $\lambda_{Eeff} = \lambda_{Meff} / \lambda_m = 1.1$
- SAE scaling: $\lambda'_{Eeff} = \lambda_{Meff} / \lambda_x^3 = 1.0$

Should these values were true, the modulus of elasticity of pediatric tissue would be similar to that of adult tissue or even stiffer, and this conclusion does not seem plausible accordant with to date published data (Franklyn et al., 2007). And even if a better prediction of the peak moment was achieved, there are still differences in the relaxation behavior between the actual and predicted pediatric response.

The study reports results on four different subjects: two adults and two children. Despite the limited sample size, this study contributes to the existing literature in presenting experimental data on the dynamic behavior of the human thoracic spine in bending for the first time. Moreover, there is no data on the dynamic behavior of the pediatric thoracic spine currently available in the literature. However, the major contribution of this research is the comparison between pediatric and adult subjects tested in the same conditions. Franklyn et al. (2007) pointed out the scarcity of pediatric biomechanical data and how more experiments were needed to assess the accuracy of currently used scaling techniques. In agreement with the results of Kent et al. (2009) for the chest, this paper shows the limitations of the scaling techniques to predict the mechanical response of the pediatric thoracic spine.

This study covers a range of results and hopefully provides the seed to foster further investigation of the mechanics of the thoracic spine. Future studies should include a greater number of specimens and increase the amplitude of the motion to facilitate the analytical modeling of the behavior of the tissue. Also, given the difficulties found to approximate the pediatric response using conventional scaling techniques, any attempt of characterizing the behavior of the developing thoracic spine should be based on experimental data from pediatric specimens.

CONCLUSION

Dynamic bending tests were performed on four pediatric and four adult thoracic FSU. After a battery of step-and-hold tests, the specimens were exposed to an increased rotation until failure of the tissue. Both the upper-thoracic and the mid-thoracic sections of the youngest specimen exhibited the lower tolerance to a bending moment, with no significant reduction in the relative angle formed by the vertebrae of the FSU. Except for one subject, the mid-thoracic sections bore greater rotations before failure than the upper sections. As part of the study, two different scaling paradigms were assessed (mass scaling, SAE scaling). The pediatric response predicted by either method never described correctly the actual pediatric behavior in the sub-failure dynamic tests. To the authors' knowledge this is the first study reporting the dynamic response of the human thoracic spine in

bending as well as comparing the response between adult and pediatric specimens.

ACKNOWLEDGMENTS

The authors would like to thank Matt Kindig, Mark McCardell and Jim Bolton for their assistance in the design of the fixture and the experimental setup.

REFERENCES

AAAM. The Abbreviated Injury Scale 2005. Association for the Advancement of Automotive Medicine, Barrington, IL, 2005.

Anderson, A. L., McIff, T. E., Asher, M. A., Burton, D. C., and Glattes, R. C. (2009). The effect of posterior thoracic spine anatomical structures on motion segment flexion stiffness. Spine (Phila Pa 1976.), 34(5), 441-446.

Ash J, Sherwood C, Abdelilah Y, Crandall J, Parent D, Kallieris D (2009) Comparison of anthropomorphic test dummies with a pediatric cadaver restrained by a three-point belt in frontal sled tests. Proc 21st Enhanced Safety of Vehicles (ESV) Conference Stuttgart, Germany

Arbogast KB, Balasubramanian S, Seacrist T, Maltese MR, Hopely T, Constans E, Lopez-Valdes FJ, Kent R, Tanji H, Higuchi K (2009) Comparison of kinematic responses of the head and spine for children and adults in low-speed frontal sled tests. Stapp Car Crash Jorunal, Vol. 53, pp. 329-372.

Belwadi A, Yang K (2008) Cadaveric lumbar spine responses to flexion with and without anterior shear displacement. IRCOBI Conference. Bern (Switzerland).

Center for Applied Biomechanics. Protocol for the Handling of Biological Material. Version 4.3. University of Virginia, 2006.

Clarke, E. C., Appleyard, R. C., and Bilston, L. E. (2007). Immature sheep spines are more flexible than mature spines: an in vitro biomechanical study. Spine (Phila Pa 1976.), 32(26), 2970-2979.

Eppinger RH, Marcus JH, Morgan RM (1984) Development of dummy and injury index for NHTSA's thoracic side impact protection research program. SAE Technical Paper Series 840885. Society of Automotive Engineers, Warrendale, PA.

Franklyn M, Peiris S, Huber C, Yang K. (2007) Pediatric material properties: a review of human child and animal surrogates. Critical Reviews in Biomedical Engineering, 35(3-4):197-342.

Green NE, Swiontkowski MF. (1998) Skeletal trauma in children. Vol III. Saunders Company, Pennsylvania.

Holmes J (2001) Epidemiology of thoracolumbar spine in blunt trauma. Acad Emerg Med 8:866-872.

Hu R, Mustard C, Burns C (1996) Epidemiology of incidental spinal fracture in a complete population. Spine 21:492-499.

Kent R, Salzar R, Kerrigan J, Parent D, Lessley D, Sochor M, Luck J, Loyd A, Song Y, Nightingale R, Bass CR, Maltese M (2009a) Pediatric thoracoabdominal biomechanics. Stapp Car Crash Journal. Vol 53:373-401.

Kent, R, Bass, C, Woods, W, Sherwood, C, Madeley, N, Salzar, R, Kitagawa, Y. (2003) Muscle tetanus and loading condition effects on the elastic and viscous characteristics of the thorax. Traffic Injury Prevention; 4(4):297-314.

Kinzel G, Hall A, Hillberry B (1972) Measurement of the total motion between two body segments-1. Analytical development. J Biomechanics 5:93-105.

Lopez-Valdes F, Forman J, Kent R, Bostrom O, Segui-Gomez M (2009) A comparison between a child size PMHS and the Hybrid III 6 YO in a sled frontal impact. Annu Proc Assoc Adv Automot Med 53:237-46

Lopez-Valdes F, Lau A, Lamp J, Riley P, Lessley D, Damon A, Kindig M, Kent R, Balasubramanian S, Seacrist T, Maltese M, Arbogast K, Higuchi K, Tanji H (2010) Analysis of spinal motion and loads during frontal impacts. Comparison between PMHS and ATD. Annu Proc Assoc Adv Automot Med 54:61-78.

Lucas, S., Bass, C., Salzar, R., Oyen, M., Planchak, C., Ziemba, A., Paskoff, G. (2008) Viscoelastic properties of the cervical spine under fast strain rate deformations. Acta Biomaterialia 4(1):117-125.

Markolf RL (1970) Stiffness and damping characteristics of the thoracic-lumbar spine. Proc. Workshop on Bioengineering Approaches to the Problems of the Spine. NIH.

McElhaney JH, Doherty BJ, Paver JG, Myers B, Gray L (1988) Combined bending and axial loading responses of the human cervical spine. SAE paper No. 881709. Society of Automotive Engineers, Warrendale, PA.

Mertz HJ, Irwin AL, Melvin JW, Stanaker RL, Beebe MS (1989) Size, Weight and Biomechanical Impact Response Requirements for Adult Size Small Female and Large Male Dummies. SAE Technical Paper Series 890756. Society of Automotive Engineers, Warrendale, PA.

Mertz HJ, Irwin AL, Prasad P (2003) Biomechanical and scaling bases for frontal and side impact injury assessment reference values. Stapp Car Crash Journal, Vol. 47, pp. 155-188.

Nahum A, Melvin J (eds) (2002) Accidental Injury, biomechanics and prevention, 2nd edn. Springer Verlag, Injury to the Thoracolumbar spine and pelvis, by A.I. King.

Nightingale RW, Chancey C, Ottaviano D, Luck J, Tran L, Prange M, Myers BS (2007) Flexion and extension structural properties and strengths for male cervical spine segments. J Biomech 40(3):535-42.

Panjabi M, Brand R, White A (1976) Three dimensional flexibility and stiffness properties of the human thoracic spine. Journal of Biomechanics 9:185-192.

Pape E, Brox J, Hagen K, Natvig B, Schirmer H (2007) Prognostic factors for chronic neck pain in persons with minor or moderate injuries in traffic accidents. Accid Anal Prev 39(1):135-146.

Shaw G, Crandall J, Butcher J (2000) Biofidelity evaluation of the Thor advanced frontal crash test dummy. In: IRCOBI Conference on the Biomechanics of Impact.

Shaw G, Kent R, Sieveka E, Crandall J (2001) Spinal kinematics of restrained occupants in frontal impacts. In: IRCOBI Conference on the Biomechanics of Impact.

Sherwood, C. P., Shaw, C. G., Van, R. L., Kent, R. W., Crandall, J. R., Orzechowski, K. M., Eichelberger, M. R., and Kallieris, D. (2003). Prediction of cervical spine injury risk for the 6-year-old child in frontal crashes. Traffic. Inj. Prev., 4(3), 206-213.

Spitzer, W. O., Skovron, M. L., Salmi, L. R., Cassidy, J. D., Duranceau, J., Suissa, S., and Zeiss, E. (1995). Scientific monograph of the Quebec Task Force on Whiplash-Associated Disorders: redefining "whiplash" and its management. Spine (Phila Pa 1976.), 20(8 Suppl), 1S-73S.

Sran, M. M., Khan, K. M., Zhu, Q., and Oxland, T. R. (2005). Posteroanterior stiffness predicts sagittal plane midthoracic range of motion and three-dimensional flexibility in cadaveric spine segments. Clin. Biomech. (Bristol. , Avon.), 20(8), 806-812.

Wheeldon JA, Pintar FA, Knowles S, Yoganandan N (2006) Experimental flexion/extension data corridors for validation of finite element models of the young, normal cervical spine. J Biomech 39(2):375-80.

Willems, J. M., Jull, G. A., and KF, J. (1996). An in vivo study of the primary and coupled rotations of the thoracic spine. Clin. Biomech. (Bristol., Avon.), 11(6), 311-316.

Wu G, van der Helm F, Veeger H, Makhsous M, Roy PV, Anglin C, Nagels J, Karduna A, McQuade K, Wang X (2005) ISB recommendations on definitions of joint coordinate systems of various joints for the reporting of human motion - part ii: shoulder, elbow, wrist and hand. J Biomechanics 38(5):981-992

Appendix I- FIXTURE DESIGN. MOMENT CALCULATION

The fixture used in the experiments described in this manuscript was designed to apply a controlled rotation to the ends of the specimens and measure the subsequent generated moments at both locations. The following paragraphs describe the process followed to calculate the magnitude of the moments.

Figure 1 showed the test fixture as well as the instrumentation used in the experiments. The free body diagram of the fixture is shown in Figure I.1

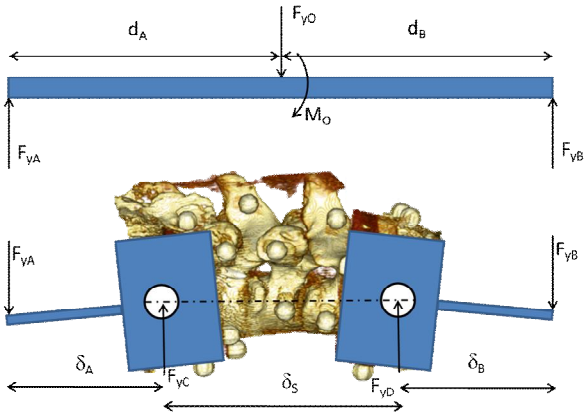

Figure I.1 Free body diagram of the fixture.

All the distances in Figure I.1 were measured by the VICON system. The reactions F_{yA} and F_{yB} are the only forces that contribute to the moment generated at the pin joints C and D in the diagram above. The moment arms (δ_A and δ_B) were also measured during

the tests. There is no horizontal force in the fixture due to the use of linear bearings connecting the fixture to the INSTRON crosshead and to the INSTRON table. F_{yC} and F_{yD} were measured directly by the two load cells. Therefore, the calculation to know the moment generated into the specimen relied only on obtaining the expression of F_{yA} and F_{yB} in terms of the known forces and distances. In the quasi-static case, these relationships can be easily obtained from the static equilibrium:

$$F_{yA} + F_{yB} = F_{yC} + F_{yD}$$

$$F_{yA} = \frac{F_{yD}\delta_B + F_{yC}(\delta_B + \delta_S)}{\delta_B + \delta_S + \delta_A} \qquad \text{Equation I.1}$$

However, the results presented in this manuscript correspond to dynamic tests and therefore Equation I.1 might not be valid in this case. The following analysis shows that the contribution of the inertia of the specimen to the calculation of the forces is so small that the equations derived for the quasi-static conditions can still be used in the dynamic case. Figure I.2 shows the free body diagram corresponding to one of the rotating cups, considering the reactions of the specimen on the cup.

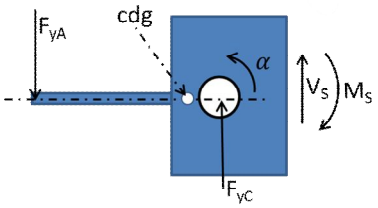

Figure I.2 Free body diagram of the fixture.

In the dynamic case, the equations of motion are given by Equation I.2, where V_s and M_s are the shear and moment reactions of the specimen on the cup:

$$F_{yA} - F_{yC} - V_s = m\ddot{y}_{cdg}$$

$$F_{yA}\delta_A - V_s\delta + M_s = I_{cdg}\alpha \qquad \text{Equation I.2}$$

The total mass of the cup and the lever is 0.114 kg and a representative value of the vertical acceleration of the center of gravity of the assembly is about 0.00525 m/s^2 (the distance between the pivot C and the center of gravity of the assembly is 3 mm). The magnitude of the inertial contribution to the force equation is several orders of magnitude smaller than the resolution of the load cell and can be neglected. A similar reasoning can be applied to the inertial term in the moments equation (I_{cdg}=3.32e-4 kgm^2; α=67.7 rad/s^2) and again the inertia contribution to the moments equation is several orders of magnitude smaller than the contribution of the other moments. Thus, the effect of the inertia of the specimen can be neglected in both equations in Equation I.2 and the expressions to calculate F_{yA} and F_{yB} given in Equation I.1 are valid. These expressions allow calculating the moment generated in the specimen by the rotation of the cups.

The nature of the specimen (involving four joints: two intervertebral discs and two facet joints) caused that specimens were subjected also to shear loads. However, Equation I.2 can also help to estimate the magnitude of the shear applied to the specimen as the difference between F_{yA} and F_{yC}. Figure I.3a and b compare the magnitude of the estimated moment ignoring the effects of the shear and the moment including the moment given by the shear load in two different tests for specimen M485. It can be seen that the effect of the shear on the calculation of the moment is negligible.

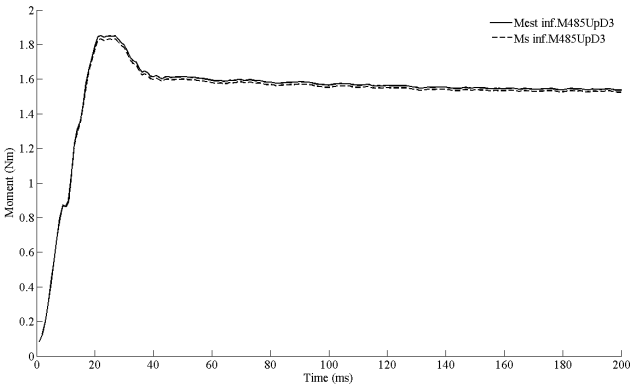

Figure I.3a Comparison between the moment applied to the specimen M485 T2-T4 in experiment D3. The solid line is the estimated moment ignoring the contribution of the shear load. The dashed line considers the contribution of the shear to the moment.

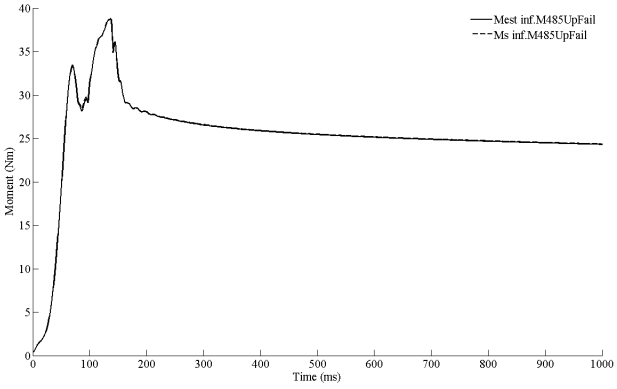

Figure I.3b Comparison between the moment applied to the specimen M485 T2-T4 in the failure test. The solid line is the estimated moment ignoring the contribution of the shear load. The dashed line considers the contribution of the shear to the moment.

Appendix II- AIS 2005 CODES OF INJURIES

Although the injuries observed in the failure tests were described in Table 4, AIS codes for each specific injury were not reported there for the sake of simplification. Table II.1 presents the AIS 2005 update codes (AAAM, 2005) of the injuries obtained in the failure tests.

Table II.1 AIS (2005 review) codes of the injuries obtained in the failure tests (IS: interspinous ligament; SS: supraspinous ligament; PLL: posterior longitudinal ligament).

	Injury	AIS 2005 codes
F470 T2-T4	IS and SS T2-T3 complete tear, partial facet dislocation T2-T3	650484.1, 650484.1, 650412.3
F470 T7-T9	IS and SS T7-T8 complete tear, flavum ligament T7-T8, bilateral facet dislocation T7-T8	650484.1, 650484.1, 650484.1, 650412.3
M485 T2-T4	Superior end cast fractured with no apparent injury.	NA
M485 T7-T9	T8-T9 disc rupture, T9 pedicle fracture, PLL rupture at T9 level	650416.2, 650426.3, 650484.1
M319 T2-T4	IS and SS T2-T3 complete tear, flavum ligament torn T2-T3, bilateral facet dislocations T2-T3	650484.1, 650484.1, 650484.1, 650412.3
M319 T7-T9	IS and SS T7-T8 complete tear, flavum ligament T7-T8, bilateral facet dislocation T7-T8	650484.1, 650484.1, 650484.1, 650412.3
M320 T2-T4	IS and SS T2-T3 complete tear, flavum ligament torn T2-T3, bilateral facet dislocations T2-T3	650484.1, 650484.1, 650484.1 650412.3
M320 T7-T9	T9 pedicle fracture, partial PLL rupture at T9, T8-T9 disc rupture, partial T8-T9 facet dislocation.	650426.3, 650484.1, 650416.2, 650412.3